

NMR with a Continuously Circulating Flow of Laser-Polarized ^{129}Xe

Roberto Seydoux* and Alexander Pines

Materials Sciences Division, Lawrence Berkeley National Laboratory, 1 Cyclotron Road, and the Department of Chemistry, University of California, Berkeley, California 94720

Mathias Haake and Jeffrey A. Reimer

Materials Sciences Division, Lawrence Berkeley National Laboratory, 1 Cyclotron Road, and the Department of Chemical Engineering, University of California, Berkeley, California 94720

Received: May 12, 1998; In Final Form: February 16, 1999

In this paper we describe the construction of an apparatus for optical pumping of ^{129}Xe in a circulating gas system connected to a probe for static high-field NMR. The optimal working conditions for the optical pumping under flow are explored, yielding a continuous gas flow with a steady-state spin-polarization of about 2%. It is shown that on various types of high surface area materials a steady-state of adsorbed laser-polarized xenon can be reached with polarizations of about 0.3%. NMR spectroscopy of this layer is greatly facilitated due to the renewable magnetization under the continuous-flow conditions allowing unprecedented fast detection of two-dimensional NMR experiments with laser-polarized Xe. The steady-state spin-polarization of adsorbed ^{129}Xe gives rise to cross-relaxation to surface nuclei such as ^1H and ^{29}Si . A direct spin-polarization-induced nuclear Overhauser effect (SPINOE) to heteronuclei is observed with an enhancement factor of about 20–30. A method is presented for simple modulation of the spin-polarization direction in the fringe field of the high-field magnet; this is exploited to obtain difference SPINOE spectra to highlight only the surface nuclei. Furthermore, a transfer via cross-polarization (CP) from adsorbed Xe to surface protons is demonstrated to select surface groups with reduced mobility compared to SPINOE detection.

1. Introduction

Nuclear magnetic resonance of xenon, especially of the spin $1/2$ isotope ^{129}Xe , has proven to be a very sensitive tool for the characterization of surfaces of microporous systems such as those of zeolites^{1–4} and clathrates.⁵ Some investigations were made on “outer surfaces”, as in the case of silicates,⁶ catalyst supports,⁷ or graphite,⁸ but since the surface areas are small, low signal intensities render ^{129}Xe NMR with thermal polarizations very time-consuming. In recent years, the introduction of laser-polarized xenon⁹ and helium,¹⁰ with nuclear spin-polarizations about 4 orders of magnitude higher than the Boltzmann equilibrium, brought a considerable improvement of the signal qualities, with its greatest impact on medical imaging of lungs^{11–13} and NMR spectroscopy of gases for diffusion studies.^{14–16} The large spin-polarization induced by optical pumping enabled as well the study of adsorbed xenon on systems with low surface areas ($<10\text{ m}^2$), such as molecular crystals or nanocrystals.^{17–19} It was equally possible to obtain a signal enhancement of other nuclear species brought into contact with laser-polarized xenon, either via thermal mixing as shown for ^{13}C in CO_2 ²⁰ and for protons in glass coatings,²¹ or alternatively a transfer to protons of poly(triarylcannabinol) could be achieved via high-field cross-polarization (CP).²² It was shown recently that a considerable polarization transfer to surface nuclei is obtained via cross-relaxation as well, either from adsorbed ^3He or ^{129}Xe ,²³ a mechanism dubbed SPINOE (spin-polarization-induced nuclear Overhauser effect (NOE)),

first observed for ^{129}Xe dissolved in benzene²⁴ and very recently with a much higher efficiency for molecules dissolved in liquid laser-polarized xenon.^{25,26} The apparent advantage of SPINOE is that double-resonance can be avoided.

Despite the importance outlined above, a widespread application of laser-polarized xenon in materials and surface science has not taken place, primarily because the polarization reservoir is subject to relaxation, preventing repetition of pulse sequences with the same starting conditions, a necessary condition for most modern NMR pulse techniques. Long-term accumulation of small polarization transfer signals induced by SPINOE is also not feasible with “single batch” experiments. The time dependence of the magnetization of surface nuclei (spins S) being in dipolar contact with a nonrenewable amount of adsorbed ^{129}Xe (spins I) follows from the Solomon equations²⁷ and is given by

$$\frac{S_z(t) - S_0}{S_0} = -\frac{\gamma_I I(I+1)}{\gamma_S S(S+1)} \frac{\sigma_{SI}}{\rho_S - \rho_I} \{e^{-\rho_I t} - e^{-\rho_S t}\} \frac{I_{zi} - I_0}{I_0} \quad (1)$$

where S_0 and I_0 are the Boltzmann magnetizations, I_{zi} is the ^{129}Xe magnetization at time $t = 0$, σ_{SI} is the cross-relaxation rate, and ρ_S and ρ_I are the self-relaxation rates of the nuclear species I and S, respectively. σ_{SI} has been assumed to be small with respect to the self-relaxation rates, and $\rho_S \neq \rho_I$. In the case where relaxation of the surface nuclei is fast compared to that of ^{129}Xe , i.e., $\rho_S \gg \rho_I$, the S-magnetization builds up with a rate corresponding to ρ_S , reaches a maximum with a value of about

* Present address: Bruker AG, Industriestrasse 26, 8117 Fällanden, Switzerland. Fax: +41 1 825 9354. E-mail: roberto.seydoux@bruker.ch.

$$\frac{S_z^{\max} - S_0}{S_0} \approx -\frac{\gamma_I I(I+1) \sigma_{SI} I_{zi} - I_0}{\gamma_S S(S+1) \rho_S I_0} \quad (2)$$

and decays toward the equilibrium value with the rate ρ_I . The validity of this behavior has been shown experimentally for protons on silica surfaces.²³ If, in contrast, the relaxation of the ^{129}Xe is faster than for the surface nuclei, $\rho_I \gg \rho_S$, the self-relaxation rate in eq 2 has to be replaced by ρ_I . Experimentally, the relaxation times for adsorbed Xe are never found to be longer than a few tens of seconds. As a consequence, the signal enhancement of a surface nucleus with relaxation times on the order of 100 s remains in the range of about 10% of the value that could be reached if the magnetization of the ^{129}Xe would not decay. Under steady-state conditions, the S -spins would reach a constant value given by eq 2 within a time on the order of $(1/\rho_S)$, provided that I_{zi} and S_z^{\max} are replaced by their steady-state values $\langle S_z \rangle$ and $\langle I_z \rangle$.

In this article, we describe the development of a closed gas-circulation system, capable of producing a steady flow of optically pumped xenon that can be used for high-field NMR with minimal time restriction. A steady state of highly spin polarized adsorbed xenon is achieved on high surface area materials. At first, this greatly facilitates ^{129}Xe NMR spectroscopy itself, allowing temperature-dependent studies and the application of 2D spectroscopy, all with the benefit of excellent signal-to-noise even with single scans and low xenon partial pressures. The steady-state adsorbed layer of polarized ^{129}Xe can be used to modulate by either SPINOE or CP the magnetization of surface protons in dipolar contact with the xenon, or a subsequent CP step transfers the polarization to adjacent heteronuclei such as ^{29}Si or ^{13}C . With the advent of steady flow, NMR experiments are facilitated due to the possibility of signal accumulation and phase cycling. Moreover, it is shown that the constant flow of spin-polarized xenon leads to a direct SPINOE to ^{29}Si nuclei on fumed silica surfaces, a nondetectable effect by any previous method, because of the long relaxation time of ^{29}Si compared to the one of the adsorbed xenon.

2. Method and Materials

2.1. Optical Pumping in a Circulating Gas System.

Previous studies²³ showed that an efficient polarization transfer through SPINOE to surface nuclei could be achieved by adsorbing approximately one monolayer of laser-polarized xenon gas on the material. With a typical sample surface of 30 m², ca. 1.5×10^{20} Xe atoms are needed and assuming a relaxation time on the order of 30 s, these would have to be replaced within 10 s in order to maintain a sufficient steady-state polarization under flow conditions. With "conventional" optical pumping by a 1 W Ti:sapphire laser, the pumping cell size is restricted to a volume of typically 30 mL, and for the pumping to be efficient, xenon pressures may not exceed about 300 Torr. These boundaries would require an optical pumping time on the order of 20 s. From the incident photon flux and the Rb spin destruction rate mainly due to collisions with Xe atoms,²⁸ it is readily estimated that the Rb density in the cell cannot exceed 2.6×10^{12} atoms per cm³ (assuming a cell length of about 5 cm). This corresponds to a cell temperature of about 90 °C. Unfortunately, with such low Rb densities the spin-exchange time is approximately 8 min,²⁸ and therefore 50 times longer than needed for flow conditions. This problem can only be solved by increasing the Rb density and the laser power by the same factor. This requires higher pumping temperatures and

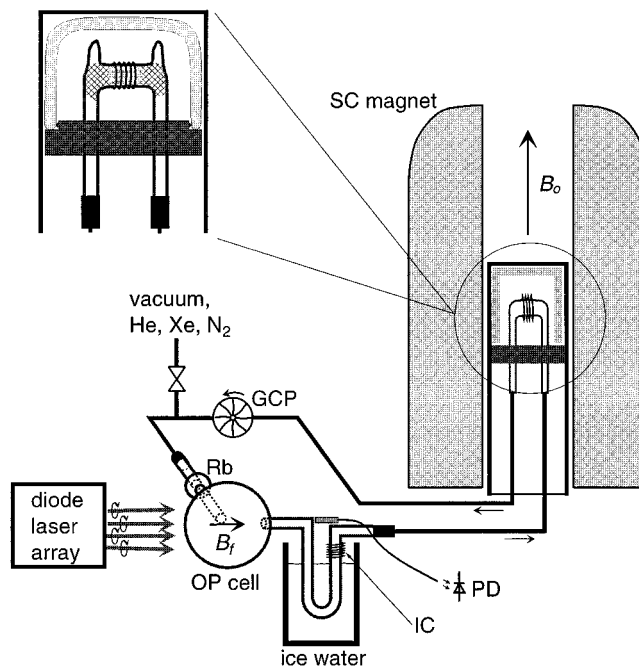


Figure 1. Experimental setup. The optical pumping cell (OP cell) is placed in the fringe field of a superconducting NMR magnet (SC magnet) at a field strength $B_f \approx 260$ G. The OP cell and the rubidium reservoir (Rb) are housed in a thermostating oven, which is not shown. The spectrum of the transmitted laser light is picked up with an optical fiber, attached to a monochromator and photodiode (PD). GCP denotes the gas-circulation pump working in the back line of the system after the gas mixture has passed the sample (checked regions are glass wool stops), which is located in a dewared region (see enlarged region) of the high-field magnet ($B_0 \approx 4.2$ T, $\omega(^1\text{H}) = 178.0$ MHz, $\omega(^{129}\text{Xe}) = 49.2$ MHz, $\omega(^{29}\text{Si}) = 35.4$ MHz). IC depicts the RF coil used for adiabatic inversion of the Xe magnetization.

the use of a high-power laser diode array. This is the key element in the experimental setup shown in Figure 1, delivering 120 W of light power at 795 nm with a half-width of about 2.5 nm using a current of 22 A and a chiller temperature of 10 °C (Optopower Corp., Model OPC-A150-795-RPCZ). The circularly polarized light is generated by 10 vertical bars of stacked diodes, resulting in a very inhomogeneously illuminated rectangle of about 1 in. \times 1.5 in. in size. The high power can only be exploited if the Rb absorption line is pressure broadened with ^4He gas.⁹ The whole gas-circulation system should therefore stand pressures up to 10 atm. The optical pumping cell as well as the sample tube in the home-built high-field NMR probe are therefore made from heavy-walled Pyrex glass (2 to 3 mm wall thickness). The glass system for the OP cell consists of a smaller sphere at the inlet, filled with some glasswool immersed in Rb metal, where the gas stream takes up the necessary amount of Rb vapor. After flowing into the actual light-irradiated compartment, which is designed as a sphere with ~ 30 mL volume, the Rb is trapped in a U-tube cooled by ice water. The two spheres are located in a small oven heated by a stream of hot air. This part of the setup is placed in the fringe field of the superconducting NMR magnet, where the field direction is approximately horizontal and about 260 G. The gradients are fairly strong with about 15 G/cm, but an estimation shows that the diffusion at the high gas pressures is sufficiently slow to avoid substantial relaxation effects within the envisaged short spin exchange times of a couple of 10 s. The optical pumping cell is connected via $1/8$ in. copper tubing to the NMR probe, leading to a dewared sample region contained in a Pyrex glass tube. The sample is held in place by glass wool stops, and the tube is flame sealed on top. All copper/glass joints are

glued, in the dewar region by low-temperature epoxy and near the pumping cell by a high-temperature epoxy. The back line contains a magnetically coupled gas-circulation pump capable of producing a 150 mbar differential pressure drop at 10 atm (Model GK-M07, Thomas Industries, WI). The whole system is evacuated to about 10^{-5} Torr prior to loading with the gas mixture. All of them are of high-purity grade (less than 0.005% impurities) and are used without further purification. The sample temperature is measured about 2 cm away from the sample tube. Systematic errors are estimated to be less than 3 °C. The temporal stability is ± 1 °C.

The performance of the system was first tested by monitoring the ^{129}Xe signal intensities of the gas at room temperature. The results of experiments, showing in detail the dynamics of the flow and optical pumping, are depicted in Figure 2. Since the system does not include a flow meter, the gas flows are measured at 1 atm, when the system is opened. The flow, indicating the volume at the actual pressure, is therefore only an estimate, since the pump performance drops slightly at higher gas pressures. In Figure 2a the Xe gas signal is monitored under a constant gas flow but with the laser being switched off and on. Since the sample space is refreshed on a time scale of a few seconds (sample volume ~ 4 mL, flow 2 mL/s), the measured time dependence reflects mainly the polarization of the optical pumping cell, delayed by the transport time and somewhat decreased by relaxational processes on the way to the sample space. In the case of a laminar gas flow in the optical pumping cell, the signal decrease and increase are independent of the flow speed and should ideally be given by exponential laws with a time constant τ corresponding to the spin-exchange time T_{ex} . However, a corresponding experiment with doubled gas flow shows time constants almost half the present value of about 7 s. This can be explained by the strong convection inside the pumping cell, caused by the inhomogeneous laser beam and the corresponding temperature variations. This leads to a time dependent overall polarization, which is also affected by the rate with which the pumping cell is refreshed with gas. The time constant τ is then given by $1/\tau = j/V_p + 1/T_{\text{ex}}$, where j is the gas flow and V_p is the volume of the optical pumping cell. Using the known values for j (~ 2 mL/s) and V_p (~ 30 mL), we calculate a spin exchange time of about 13 s.

Figure 2b monitors the Xe signal intensity after a stopped flow. The first points are sampled when the gas-circulation pump is halted, showing the remaining polarization after the gas is kept for 3 min in the sample tube. The magnetization apparently decays very slowly, mainly because of the pulse repetition. After the pump is switched on at point A (and the laser blocked), the signal first drops, indicating an almost complete depolarization of the gas in the connection between the sample tube and the OP cell. This is most likely caused by diffusion in the strong field gradients and also by wall collisions in the copper lines. The drop and the following rise in signal are characterized by the gas flow j and the sample volume size V_s , i.e., the rate with which the sample space is emptied or filled with polarized gas. The subsequent decay should be reflected by the decay of polarization in the optical pumping cell, which was left dark at point A, that is again an exponential behavior with the constant $1/\tau = j/V_p + 1/T_{\text{ex}}$. The experimentally determined value for τ of 12 s is longer than in the experiment of Figure 2a. This is caused by the slightly smaller gas flow and by the longer spin-exchange time within the cell that has been left in the dark for almost a minute. Thereby the temperature in the OP cell decreased, since the laser heats the thermostating housing of the cell. The same "pump on/light off experiment" with shorter

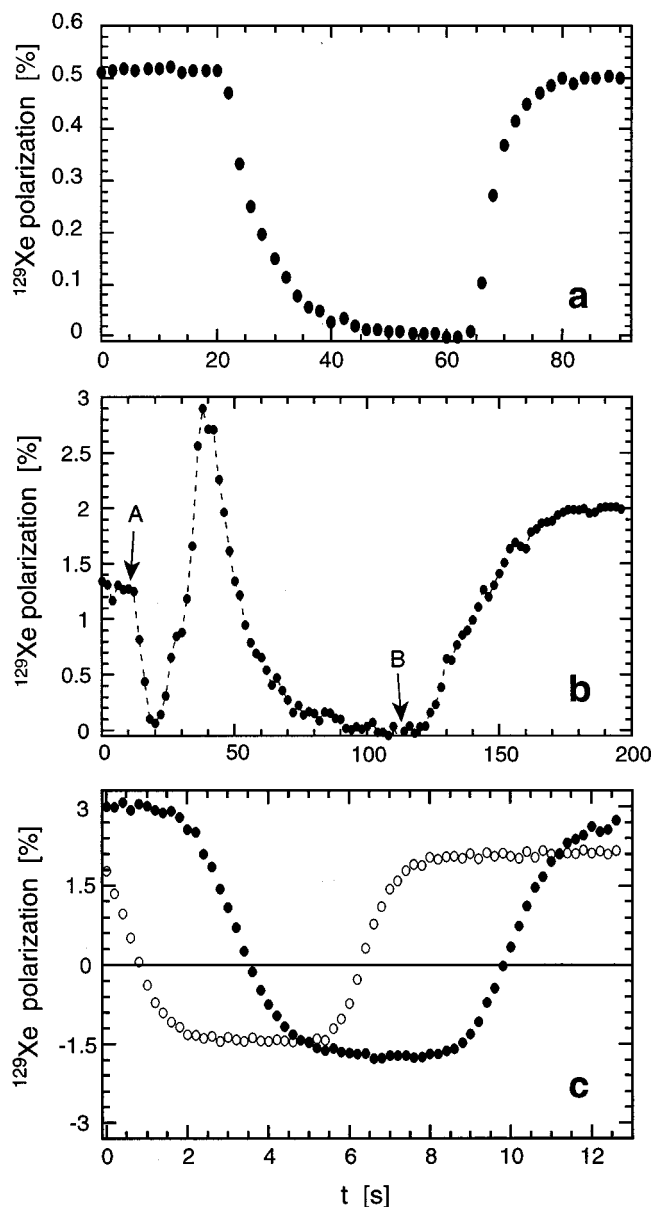


Figure 2. Spin-polarization of gaseous ^{129}Xe at room temperature. (a) A constant gas flow of 120 mL/min is applied. Around 20 s the laser beam is blocked and the irradiation is resumed at about $t = 60$ s. The ^{129}Xe signal is monitored by 5° tip angle pulses. The gas mixture is composed of 300 Torr natural abundance Xe and 100 Torr N_2 and pressurized with helium (^4He) to 1.5 atm. The optical pumping cell temperature is 190 °C. (b) The gas-circulation pump is halted for 3 min and then switched on at the seventh pulse while the laser is shuttered (arrow at A). The resulting gas flow amounts to ≈ 100 mL/min. The laser irradiation is resumed after about 2 min at point B. The gas mixture consists of 340 Torr natural abundance xenon and 120 Torr N_2 pressurized with helium to a total pressure of 9 atm. The signal is detected with 5° tip angle pulses. The optical pumping runs at 180 °C. (c) Effect of adiabatic inversion in the fringe field. Between -6 s $< t < 0$ s a RF of 450 kHz with a peak field $B_1 \approx 10$ G is irradiated. The ^{129}Xe signal is then sampled with 8° tip angle pulses. Full symbols are taken with a flow of 24 mL/min and open ones with 55 mL/min. The total pressure is 4 atm.

light irradiation times (1 min or 30 s) yielded about the same height for the maximum polarization, indicating that the spin-exchange time in the light-irradiated cell is in fact faster than 30 s, but the dip prior to the rise is smaller, because the gas in the connection apparently does not relax so much during the shorter stopped-flow times. At point B the laser irradiation is resumed. The following rise is slower than measured in Figure

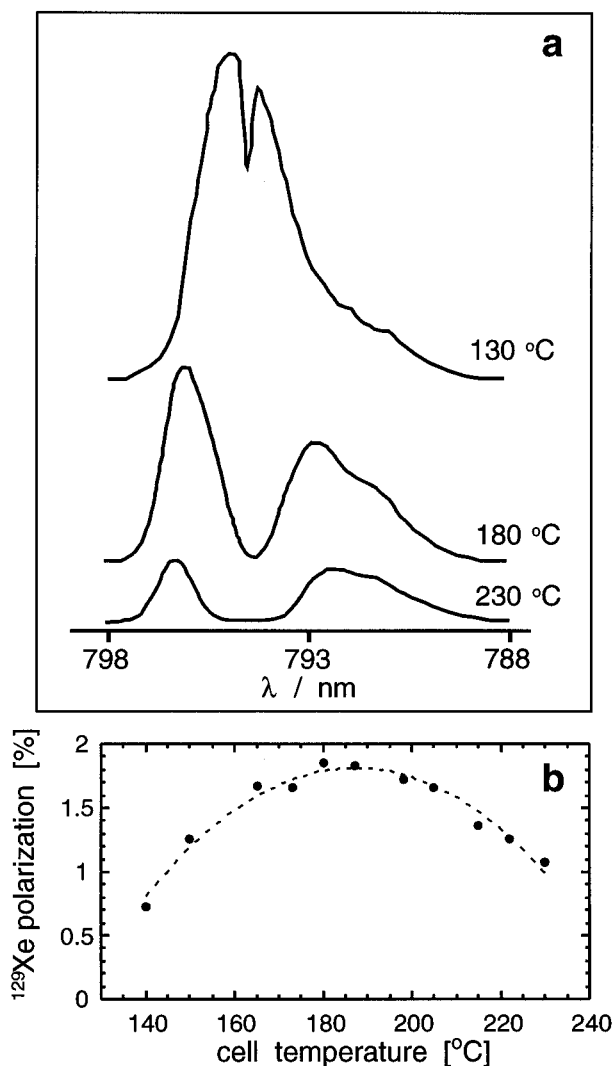


Figure 3. (a) Light absorption profiles as measured after the optical pumping cell at different cell temperatures. The intensities are only qualitatively to scale. (b) Spin-polarization of ^{129}Xe in the gas at room temperature as a function of the optical pumping cell temperature under a constant flow rate of 100 mL/min (300 Torr natural abundance Xe, 100 Torr N_2 , 3 atm total pressure).

2a. This is again caused by the fact that the cell cooled to about 120 °C while remaining in the dark for 2 min. The temperature is then slowly restabilized at about 180 °C with the aid of the laser irradiation. After about 3 min a steady-state polarization is reached around 2%. This value is smaller than the one reached in the maximum of the preceding stopped-flow experiment, most probably caused by a different Rb distribution under flow. Parts a and b of Figure 2 give a qualitative picture of the dynamical behavior in the present setup. A quantitative description of the evolution of polarization under variable conditions, however, is far from trivial and the efficacy of such a description is unclear.

The optimal working conditions for the optical pumping are monitored by the Rb absorption line shape, as shown in Figure 3a. The comparison of the steady-state polarization, shown in Figure 3b, with the corresponding absorption curve clearly demonstrates the key feature. The light at resonance is just fully absorbed, but not “clipped” as at 230 °C, where the back part of the cell remains dark. At higher temperatures the apparent width of the absorption dip is several times larger than the pressure broadened width of the resonance (about 0.15 nm at 3 atm helium pressure), since the absorption length becomes much

shorter than the length of the cell.³⁶ In the present setup we do not observe a substantial improvement of the polarization when working with helium pressures higher than about 4 atm. Additionally, the spin-polarization drops when higher xenon partial pressures are used. Good results are still obtained at 300–400 Torr.

For difference measurements involving spin-polarization transfer there are several possibilities: (i) RF modulation of the Xe polarization at high field, as demonstrated earlier,²⁹ (ii) laser irradiation off/on, (iii) inversion of the polarization in the fringe field. Method i needs a ^{129}Xe RF channel in the probe and the lifetime of the inverted state is limited by the gas flow; (ii) has an inherent smaller dynamic range and is slow, since the temperature of the optical pumping cell is affected by the procedure; the most convenient last possibility could be achieved by inverting the direction of the fringe field. This would require a special magnet coil with fairly high currents for producing about 300 G in the cell region, resulting in the need for high mechanical strength. The next straightforward way would be to change the circular polarization of the pumping light by means of a $\lambda/2$ -plate, periodically introduced into the beam. However, such a plate would have to cover the entire beam area of about 1.5 in.² and is therefore a very expensive solution. In view of these difficulties, we have chosen a different approach that involves an adiabatic inversion of the Xe polarization in the fringe field. The only additional elements needed are a low-frequency generator with several Watts of output power and a coil wrapped around the outlet of the Rb-trap (see Figure 1), where the fringe field is still more or less horizontal (25° tilted with a component perpendicular to the coil axis of $B_{ic} \approx 380$ G) but has a gradient of about 15 G/cm in the vertical direction. At a gas flow rate of 30 mL/min and an inner glass tube diameter of about 4 mm in the coil region, the gas speed results in 14 cm/s. The ^{129}Xe spins experience therefore a field change of $dB_{ic}/dt \approx 210$ G/s. The coil has 80 turns with an inductive impedance of about 75 Ω at a frequency of 450 kHz, the ^{129}Xe Larmor frequency at B_{ic} . Application of a peak-to-peak voltage of about 30 V results in an estimated value for the rotating field component of $B_1 \approx 10$ G. This ensures that the adiabatic condition $dB_{ic}/dt \ll \gamma_{Xe}(B_1)^2$ is fulfilled. The field sweep through the adiabatic condition is hereby provided by the gas transport itself. Figure 2c shows the result of a 6 s RF irradiation prior to the monitoring pulses. The adiabatically flipped signal shows up after 8 or 11 s depending on the gas flow. This is about the time it takes to transport the gas from the optical pumping cell to the sample space. The polarization is inverted with an efficiency of 60%. The loss is most probably caused by diffusion in the relatively strong field gradients in the fringe field. At higher gas flow the efficiency is raised to 70%. Narrowing the inner tube diameter in the coil region, which increases the flow speed in the coil area, might therefore further improve the performance. Nonetheless, this rather simple solution enables us to supply the sample in a high-field NMR magnet with a continuous-flow of laser-polarized xenon of either polarization direction, with timings that can be controlled by pulse programs of the NMR spectrometer. Figure 2c shows also the influence of the circulation speed on the steady-state polarization, which decreases slightly with increasing flow.

2.2. Materials. To study either adsorbed xenon or polarization transfer to the surface nuclei, samples based on fumed silica, AEROSIL,³⁰ were used. AEROSIL300 is hydrophilic with a nominal surface area of 300 m²/g. Packed only by shaking, the material occupies a volume of about 20 mL/g. It consists of small particles of about 7 nm diameter, clustered together in

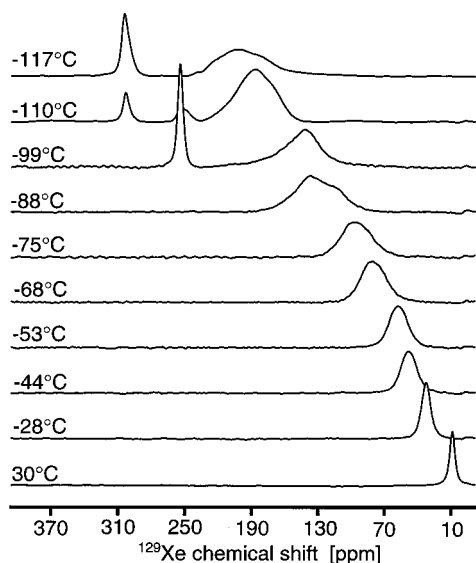


Figure 4. NMR spectra of ^{129}Xe on AEROSIL300 under continuous-flow conditions and at different sample temperatures. The gas mixture consists of 800 Torr natural abundance Xe and 100 Torr N_2 pressurized to 4.6 atm with helium. The gas flow is approximately 30 mL/min, and the spectra are recorded as single scans with a 2° tip angle. The signal is further attenuated by 10 dB.

bigger aggregates. The surface is terminated with OH groups, with an average density of 2.5 per nm^2 .³⁰ A hydrophobic variant, AEROSIL R202, has most of its OH-groups grafted with dimethylsiloxane chains, $[\text{Si}(\text{CH}_3)_2\text{O}]_n$, and its surface area is $180 \text{ m}^2/\text{g}$. For a further study CsI was chosen, where Xe is known to have increased adsorption energies vis-à-vis silica surfaces. To purify the crystal from paramagnetic impurities, it was recrystallized three times from ultrapure water, and in order to increase the surface, it is coprecipitated from an aqueous suspension containing about the same amount of AEROSIL300. This sample is potentially interesting for polarization transfer to a surface quadrupolar nucleus, ^{133}Cs , which is in a cubic bulk environment. All the samples were evacuated to a pressure better than 10^{-5} Torr for several hours; in the case of AEROSIL300 and the coprecipitated CsI mixture, additional heating to about 120°C was needed in order to remove adsorbed water.

3. Application for Surface NMR Spectroscopy

3.1. NMR of Adsorbed Xe, 2D Exchange Spectroscopy.

Figure 4 shows a stacked plot of ^{129}Xe spectra recorded as single scans at different sample temperatures on AEROSIL300. The spectra at higher temperatures consist of one single peak, which is therefore always an exchange peak between gas and the adsorbed state. The peak at 30°C appears in fact shifted by 10 ppm with respect to gas at 1 atm pressure. With decreasing temperature the exchange peak broadens and shifts toward 200 ppm. Around -100°C a second, relatively sharp line arises at 255 ppm, which we attribute to laser-polarized xenon in the liquid phase. At -110°C a third line with a shift of 304 ppm is attributed to laser-polarized solid xenon. The solid forms at a temperature slightly higher than the triple point (-113°C), probably due to uncertainties in the temperature measurement. Previous work⁶ reports a shift of 316 ppm at 77 K. The relatively large thermal expansion of solid xenon and the corresponding effect in the shift³¹ causes the discrepancy. A temperature series with a lower Xe partial pressure (300 Torr) looks similar, but the solid is only formed below -120°C , as would also be expected from the Xe phase diagram. This, together with the

fact that xenon is effectively adsorbed and exchanged in an atmosphere containing mostly helium, proves the latter to act only as a carrier gas. The spin-polarization of about 2–3% at room temperature drops for the adsorbed signal to about 0.25% at -120°C . The drop is caused by two effects: (i) shorter T_1 and (ii) slower exchange for the adsorbed xenon at lower temperatures. In a simplified model, wherein the spatial variation of the polarization over the sample is neglected, we can write the change in magnetization of the adsorbed layer as

$$\frac{dI_z^{\text{ads}}}{dt} = -\frac{I_z^{\text{ads}}}{T_1} + \frac{1}{t_{\text{ex}}}(I_z^{\text{gas}} - I_z^{\text{ads}}) \quad (3)$$

with

$$t_{\text{ex}} = \frac{kT_{\text{R}}V_{\text{S}}n_{\text{ads}}}{p_{\text{Xe}}j} \quad (4)$$

where I_z^{ads} and I_z^{gas} are the Xe magnetizations in the adsorbed phase and in the incoming gas stream, respectively (the limit has been used where these are much larger than the Boltzmann magnetizations). The small cross-relaxation can be disregarded in this concern, since it does not affect the relaxation of Xe. The number density of adsorbed xenon atoms n_{ads} is a function of the residual xenon partial pressure p_{Xe} and the sample temperature T_{S} . For eq 4 it was further assumed that most of the gas in the system is at room temperature T_{R} and that everything delivered to the sample is converted into an adsorbed state, for which the spectra show in fact evidence, since a separate gas peak is missing. The exchange time t_{ex} is the time necessary to exchange all of the adsorbed xenon. Equation 3 may be simplified to yield

$$\frac{dI_z^{\text{ads}}}{dt} = -\frac{I_z^{\text{ads}}}{\tau} + \frac{I_z^{\text{gas}}}{t_{\text{ex}}} \quad \text{with} \quad \tau = \frac{T_1 t_{\text{ex}}}{T_1 + t_{\text{ex}}} \quad (5)$$

In case the flow is stopped, the signal decays exponentially with the spin–lattice relaxation time of the adsorbed xenon, T_1 . If an inversion–recovery type experiment is performed under flow, the adsorbed signal reaches the steady polarization value $\langle I_z^{\text{ads}} \rangle / \langle I_z^{\text{gas}} \rangle = \tau / t_{\text{ex}}$ with the time constant τ . At -120°C , T_1 has been determined as 32 s and τ as 17 s. The resulting exchange time t_{ex} is 36 s and the ratio of polarizations would be expected to be 0.5. The lower experimental value of about 0.1 indicates that the polarization of the gas before it enters the sample region is probably much lower than at room temperature; this could be attributed to additional relaxation in the cold part of the probe. At a temperature of -100°C , T_1 increases to 66 s and the exchange time t_{ex} drops to only 9 s.

Figure 5 shows a temperature series of ^{129}Xe spectra on the coprecipitated mixture of CsI with AEROSIL300. In contrast to AEROSIL300, already at higher temperatures two peaks appear in addition to a separate gas peak. The shifts at -30°C are 80 and 100 ppm and hence much larger than the corresponding shift on the AEROSIL300, in which case 35 ppm is determined. At lower temperatures the signal intensity drops and the peak of solid Xe never appears. These observations support the model of a surface with much higher adsorption energy for Xe compared to that on AEROSIL300. At low temperatures all of the xenon is adsorbed and removed from the circulating gas stream. The two peaks at higher temperature might indicate the existence of a microscopic inhomogeneity of the surface. Regions with CsI and AEROSIL300 could alternate and give rise to two exchange peaks. One way to

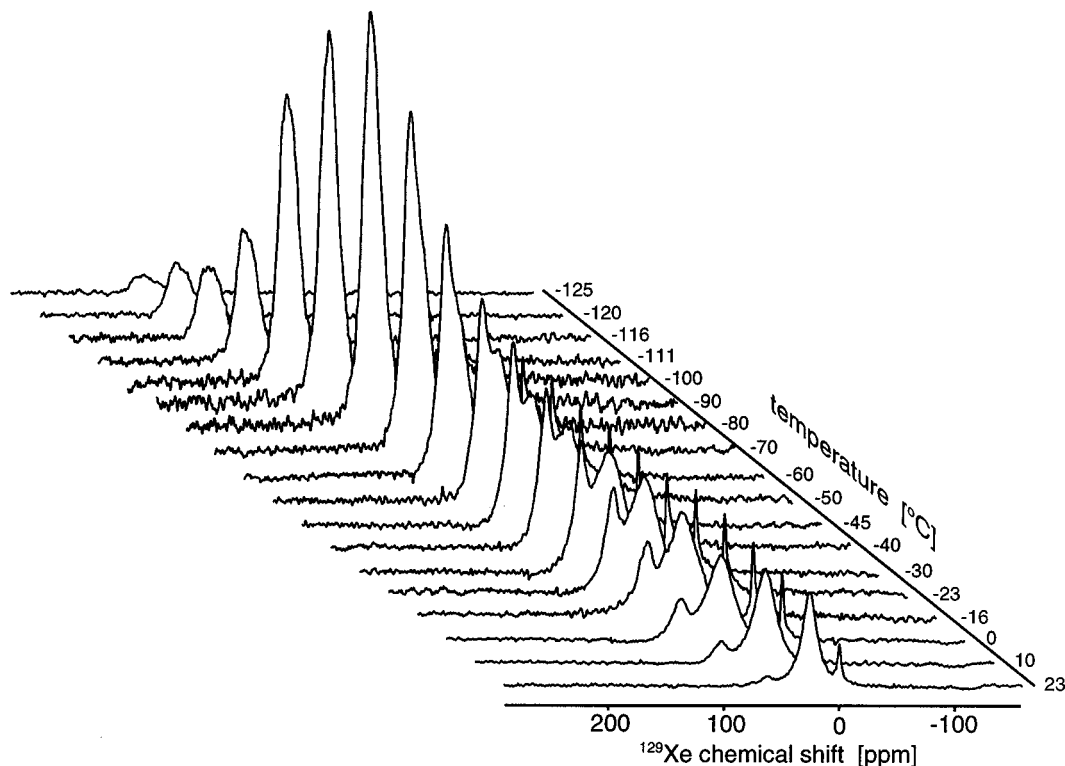


Figure 5. Temperature-dependent NMR spectra of ^{129}Xe on a coprecipitated mixture of AEROSIL300 and CsI. The gas mixture consists of 300 Torr natural abundance Xe and 100 Torr N_2 pressurized to 4 atm with helium. The gas flow is approximately 30 mL/min. The spectra are recorded as single scans with 10° (low temperature) to 60° (room temperature) tip angles and are plotted to scale. The noise therefore increases toward lower temperatures, except for the lowest ones, where up to four scans have been accumulated.

explore the exchange times between these two regions would be to apply 2D exchange spectroscopy.³² With ^{129}Xe of thermal polarization this has been applied in a number of interesting cases,^{7,33} but usually this involves very time-consuming signal averaging, leading to measurement times of several days. Furthermore, the xenon pressures are restricted to many atmospheres, so that Xe–Xe interaction may alter the line width and also the exchange behavior. As 90° pulses are needed for this type of measurement, the application of laser-polarized xenon was so far impossible. However, with the circulating-gas setup the magnetization can be fully restored after the pulse sequence and even signal averaging with phase cycling becomes possible. To demonstrate this, the sample was kept at a temperature of -15°C , where two exchange peaks appear (top left of Figure 6). With an inversion–recovery sequence under flow it is determined that the magnetization in the peaks can be fully restored after 10 s, which is then the value that sets the repetition time. A standard sequence with three 90° pulses is applied with 64 t_1 increments. The signal-to-noise is so good that spectra are recorded as single scans. No phase cycling can then be applied, but transverse magnetization during the mixing time is canceled by the fact that $t_{\text{mix}} \geq T_2$. The resulting 2D spectra with various mixing times (Figure 6) demonstrate an exchange on the order of 10 ms. A lower limit of about 1 ms is given by the existence of two distinct peaks with a spacing of about 1500 Hz. The intensities are not affected by T_1 effects, since this value is about 19 s, but instead, the sharper peak at higher shift decays very fast, which must be due to the exchange. Of course the present method is only applicable if the exchange times are short compared to the time required for replacement of the Xe. However, this does not pose very stringent restrictions. The gain in measurement time is considerable—each spectrum requires only 20 min instead of 1 week (assuming 128 scans, with $2T_1$ spacing).

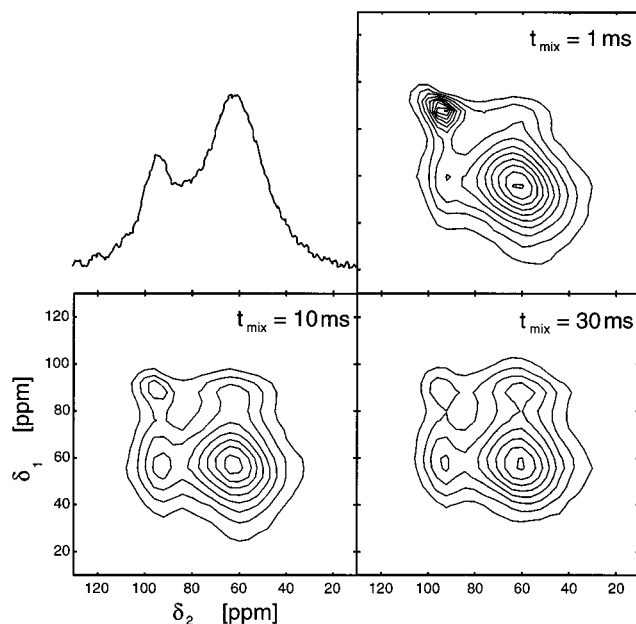


Figure 6. 2D exchange spectra of laser-polarized ^{129}Xe on the coprecipitated mixture of CsI with AEROSIL300 at a temperature of -15°C . The sequence is $[90^\circ-t_1-90^\circ-t_{\text{mix}}-90^\circ(\text{acq})]$ with 64 increments and phase-sensitive detection in the first dimension (method of States). Single scans are detected with a repetition time of 10 s. The xenon spectrum is shown in the top-left portion; 10 contour lines are drawn between 20 and 99% of the maximum height of the spectrum with $\tau_{\text{mix}} = 1$ ms.

3.2. Polarization Transfer to Surface Protons via SPINOE and CP. As already demonstrated in a previous work,²⁹ the steady-state spin-polarization of the adsorbed ^{129}Xe gives rise to a steady-state SPINOE to surface protons in silanol groups of AEROSIL300. In Figure 7 the SPINOE is plotted as a

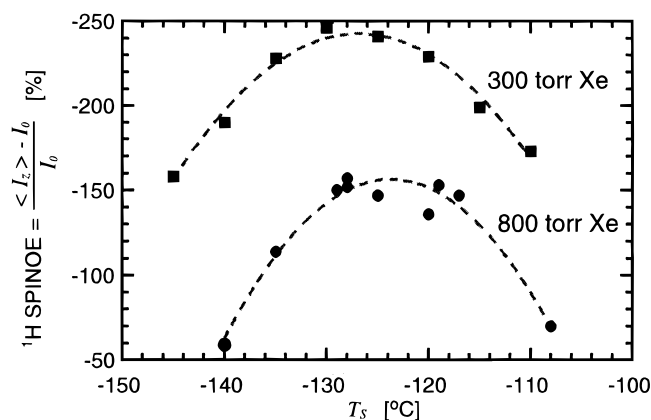
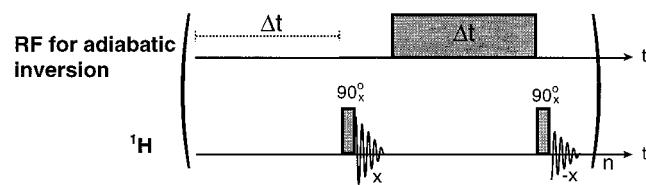


Figure 7. Steady-state proton SPINOE on AEROSIL300 as a function of sample temperature and xenon partial pressure. To the natural abundance xenon gas are added 100 Torr of N_2 and the mixture is pressurized with helium to 4.5 atm. The gas flow is about 30 mL/min.

SCHEME 1. Sequence for Difference NOE Measurements of Surface Protons



function of sample temperature and xenon partial pressures (the pressure that would result without adsorption). Both curves exhibit a maximum, the one for lower pressure being slightly shifted to lower temperatures. Qualitatively, the existence of the maximum can be understood on the basis of eqs 2, 4, and 5. The polarization in the adsorbed state is proportional to $\{T_1(\text{Xe}^{\text{ads}})p_{\text{Xe}}\}$ and inversely proportional to n_{ads} . T_1 and p_{Xe} are decreasing with falling sample temperature, and n_{ads} increases, ending in a saturation. Hence, the polarization decreases monotonically with lower temperature. On the other hand, the cross-relaxation rate is increasing since the xenon concentration is growing in the adsorbed layer and because, at the studied temperatures, we are still in the limit of short correlation times. Less important, but usually working in the same direction, is the temperature variation of the T_1 of the surface nuclei, i.e., increasing values with lower temperature. The overall lower values for 800 Torr are due to a less efficient optical pumping with higher xenon partial pressure and, especially on the lower temperature side, a large amount of polarized gas is lost in exchange with frozen Xe, which lengthens the exchange times (t_{ex}) for the adsorbed xenon, resulting in a worse adsorbed polarization (I^{ads}). The shift of the maxima might as well be due to the loss of Xe through freezing, which starts at higher temperatures in the case of higher partial pressure.

With the possibility of performing an adiabatic inversion of the xenon polarization in the fringe field, a new sequence for difference NOE measurements is possible, as explained in Scheme 1. In the first Δt period the polarization is unchanged, while in the second it is chosen in the opposite direction. The receiver phases are 180° rotated, so that only the proton signal is added that has been influenced by the polarized ^{129}Xe , i.e., the surface nuclei experiencing a SPINOE. The unaffected bulk or probe background is averaged to zero. The advantage over the earlier proposed method with Xe inversion at high field²⁹ is the equal time spacing between subsequent acquisitions, avoiding T_1 artifacts and therefore enabling the measurement of smaller NOE's. The time Δt is chosen long enough to make

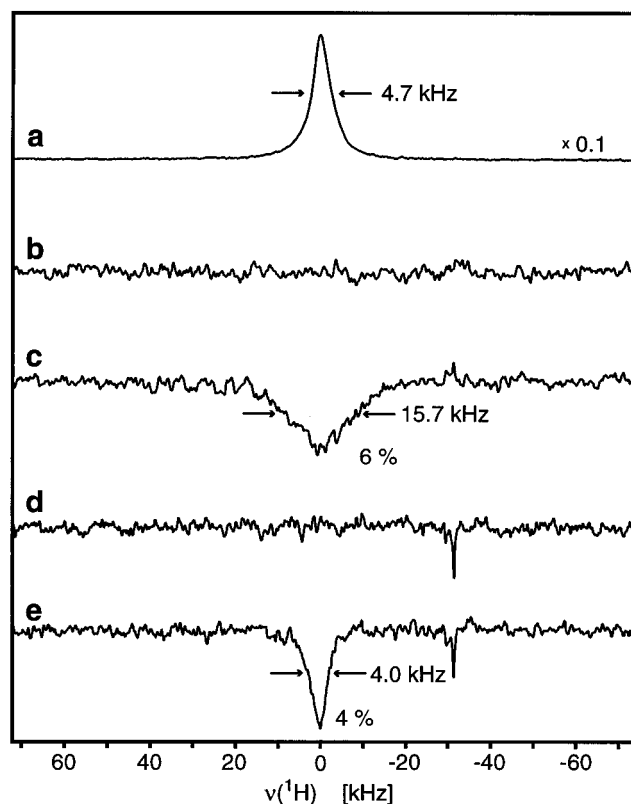


Figure 8. Proton NMR spectra of AEROSIL R202 at -110°C : (a) probe background suppressing Bloch decay, i.e., $[90^\circ(\text{acq})-0.1\text{ s}-90^\circ(-\text{acq})]$, 32 acquisitions; (b) CP from ^{129}Xe to ^1H with a contact time of 1 ms and a spin-lock field of 110 rad/s, 32 scans with a repetition time of 30 s, laser off; (c) the same as (b) but with the laser on; (d) difference SPINOE measurements according to the sequence displayed in Scheme 1, $n = 16$, $\Delta t = 40$ s, laser off; (e) the same as (d) but with the laser on. The legend marks line widths at half-height and signal intensities relative to the bloch decay (gas mixture 280 Torr natural abundance Xe, 100 Torr N_2 , 4 atm total pressure; 30 mL/min flow).

sure that the Xe on the sample has been completely exchanged by the inverted polarization. This can be monitored with an experiment similar to the one described in Figure 2c and results in a Δt of about 30 s. To this value the relaxation time of the surface nucleus has to be added to fully develop the SPINOE. In Figure 8 traces d and e demonstrate the feasibility of this method on a sample of AEROSIL R202.³⁷ The difference spectrum shows a line of about the same characteristics as the bloch decay, i.e., a relatively sharp line that is attributed to protons in still mobile parts of the dimethylsiloxane chains grafted to the silica surface. Compared with the SPINOE of protons in OH groups (see Figure 7), the effect is about 50 times smaller. This is mainly attributed to the much shorter relaxation times of the protons, being about 0.8 s versus 15 s in case of OH on AEROSIL300.

In contrast to cross-relaxation to surface protons, a CP from adsorbed Xe is also feasible, as is shown in traces b and c of Figure 8. The effect is clearly a coherent transfer since it vanishes by setting the first 90° pulse on the ^{129}Xe to zero. The polarization source is the adsorbed Xe since the effect again decreases below -120°C , where in fact solid Xe appears in the spectrum, while the adsorbed peak intensity diminishes. The CP efficiency is small if compared with enhancement factors of 70 found in earlier studies²² where the source was solid xenon. Adsorbed Xe is distributed homogeneously on the surface and the magnetization is refreshed in the circulating-flow setup without changing the sample temperature. A standard CP with phase cycling and a contact time of 1 ms ($T_{1\rho}(\text{Xe}^{\text{ads}}) \approx 2$ ms at

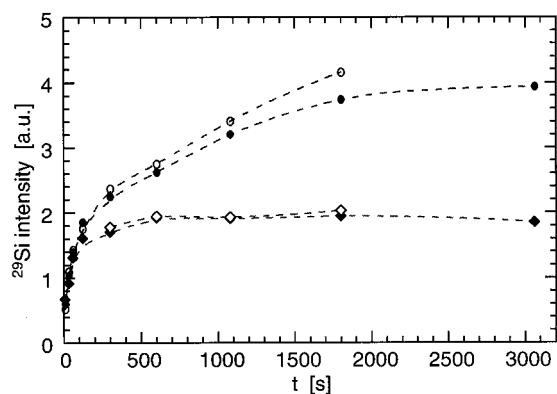


Figure 9. Effect of laser-polarized ^{129}Xe on the saturation recovery of the ^{29}Si signal of AEROSIL300. The open symbols are the results with a proton decoupling sequence during the recovery time (BLEW-12). The values are integral intensities of single scans with a 90° pulse. The sample temperature is kept at -125°C . The gas mixture consists of 300 Torr xenon enriched to 80% in ^{129}Xe and 100 Torr N_2 , pressurized to 4 atm with helium. Circles are taken with and diamonds without laser irradiation. Approximately 90% of the intensity without laser irradiation can be attributed to a ^{29}Si signal from the Pyrex glass container.

the spin-lock field strength) can therefore be applied under flow. These advantages are not present with the earlier approach involving frozen Xe, where it is difficult to create a homogeneously distributed Xe layer and where it would be necessary to heat up the sample in order to renew it. In addition, the present CP effect appears at the same temperature as the SPINOE, which allows us to compare two transfer mechanisms to the surface at exactly the same sample conditions. The key difference in the spectra is the line width—with CP a very broad line appears, whereas SPINOE highlights a narrow signal. Tentatively, we attribute this to protons of rigid and more mobile parts of the siloxane groups. As a motionally induced process, the SPINOE is more efficient on mobile surface groups, whereas CP works best if the spins are in “rigid” contact with each other. The two transfer mechanisms affect therefore motionally different surface species.

3.3. SPINOE to Surface Heteronuclei. For this experiment AEROSIL300 is chosen as a sample, but the gas system is now loaded with xenon enriched to 80% in the isotope ^{129}Xe . With a partial pressure of 300 Torr the steady SPINOE on protons of silanol groups results as -600% . This is a factor of 3 bigger than with natural abundance xenon (see Figure 7) caused by the 3-fold higher isotope density. Since the xenon can be recollected simply by circulating the mixture while the ice water of the Rb trap is replaced by liquid nitrogen, the use of expensive isotopically enriched gases poses no problem with our system. The effect of this laser-polarized xenon on the ^{29}Si signal intensity is depicted in Figure 9. The signal recovery after saturation depends on the Xe polarization, and additionally, proton decoupling yields higher intensities too. The silicon NMR signal under our static conditions is simply one line of about 26 ppm width and cannot be distinguished from the ^{29}Si signal contributed from the Pyrex sample tube containing the Aerosil. A number estimation shows that, from the thermal polarization signals (the diamonds in Figure 9), about 90% are “background” from the Pyrex tube. The curves obtained without light irradiation recover therefore faster than with the laser on, because in the former case mainly the faster relaxing ^{29}Si of the Pyrex is seen. From the remaining 10% it is estimated with the Aerosil particle size that 70% are from bulk while 30% are due to surface silicon groups, split as 10% in SiO_2 and 20% in OH groups. With this number estimation, the observed enhance-

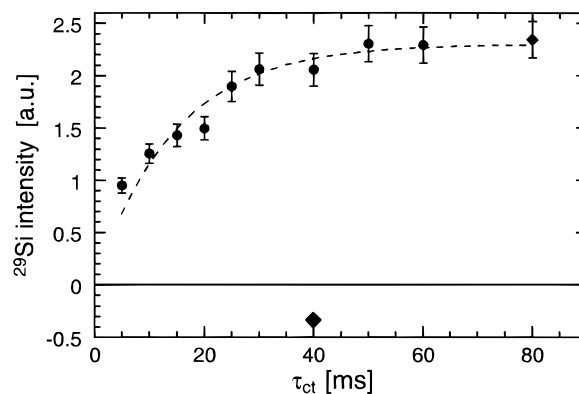


Figure 10. Integral intensities of ^{29}Si CP spectra of AEROSIL300 at -125°C . The data shown by circles are recorded with laser irradiation, and the single negative point at 40 ms denotes the CP spectrum without laser light. The optical pumping conditions are the same as described for Figure 9. Spectra are recorded by acquisition of eight CP scans with a 10 s pulse delay, a matching field strength of 110 rad/s, and saturation of the signal prior to the start of the sequence.

ment of surface ^{29}Si is between 20 and 30. The recovery under light irradiation is slower, as it is now reflected by the Aerosil ^{29}Si T_1 , which is around 1000 s. This large T_1 value is responsible for the considerable SPINOE, whose sign is opposite to the SPINOE observed on protons of OH groups. The sign demonstrates that the main contribution to the SPINOE is a direct coupling between Xe and Si. Using the above assumptions, a cross-relaxation σ_{Si} of about $3 \times 10^{-5} \text{ s}^{-1}$ is estimated from eq 2. If proton decoupling is applied during the recovery, additional intensity builds up; i.e., also a cross-relaxation from protons to silicon takes place. The proton polarization under continuous-flow SPINOE, $(\langle I_z \rangle - I_0)/I_0 \approx -6$, together with the appropriate signs for the gyromagnetic ratios results in a negative effect (see eq 2), diminishing the signal when the decoupling is not applied. At this point we cannot distinguish whether the direct SPINOE acts only on the SiO_2 or also on the Q^3 groups. This study is in progress with the SPINOE under MAS conditions³⁴ where the two groups can be spectroscopically resolved.

The steady-state enhancement of the protons can also be used to improve the signal of a CP from ^1H to ^{29}Si , as is demonstrated in Figure 10. Compared to a previous study with “one-batch” of laser-polarized xenon,³⁵ the effect can now be studied much more accurately and under signal accumulation with the appropriate phase cycling to remove residual background signals appearing in single CP scans. The enhancement is a factor of about -6 , i.e., the same as for protons. The optimum contact times for CP are rather long (~ 40 ms), which is attributed to a long $T_{1\rho}(^1\text{H})$ combined with a slow buildup (~ 14 ms) due to the small dipolar coupling between protons and silicon in Q^3 groups. Apart from speeding up or improving the quality of a measurement, the presented CP could also be performed with cycling of the Xe polarization, as was done for protons in the previous section. This could selectively highlight heteronuclei on the surface belonging to hydrogenated groups being in contact with adsorbed xenon. The direct SPINOE, on the other hand, would highlight chemical groups where xenon comes more closely into contact with the heteroatom itself.

4. Outlook

The possibility to recirculate a gas containing spin-polarized ^{129}Xe offers new ways to extend many common NMR experiments also on highly polarized species. This should greatly facilitate ^{129}Xe NMR for imaging of porous materials and aid

in the exploitation of multidimensional experiments. The effective adsorption and exchange of spin-polarized Xe carried in a helium gas stream through high surface area materials with the corresponding buildup of a steady-state, highly spin-polarized Xe layer can be exploited to highlight surface spins via difference SPINOE spectra and direct CP from adsorbed Xe. Combining the various transfer methods with intermediate CP steps offers alternative ways to differentiate surface groups by their mobility or accessibility for the adsorbed Xe. Although most of our test systems focused on spin species residing only at the surface, in which case T_1 -selective experiments could be performed as well to distinguish between chemically different surface groups, our approach with laser-polarized Xe potentially offers a way to obtain NMR spectra of the surface even in cases where it is not spectrally different from the bulk. A wider application of the technique for surface NMR spectroscopy could be expected if in the future it will be possible to work with much higher ^{129}Xe polarizations (i.e., 20% or better) and if the methods developed here are extended also to SPINOE under MAS spinning, which has already been shown to be feasible.³⁴

Acknowledgment. This research was supported by the Director, Office of Energy Research, Office of Basic Energy Science, Materials Science Division, of the U.S. Department of Energy under Contract No. DE-AC03-76SF00098. R.S. acknowledges support from the Swiss National Science Foundation, and M.H. thanks the Studienstiftung des Deutschen Volkes and the BASF-AG for a postdoc fellowship.

References and Notes

- Ito, T.; Fraissard, J. *J. Chem. Phys.* **1982**, *76*, 5225.
- Dybowski, C.; Bansal, N.; Duncan, T. *Annu. Rev. Phys. Chem.* **1991**, *42*, 433.
- Jameson, C.; Jameson, A.; Gerald, R.; de Dios, A. *J. Chem. Phys.* **1992**, *96*, 1676.
- Raftery, M. D.; Chmelka, B. F. In *NMR Basic Principles and Progress*; Bluemich, B., Kosfeld, R., Eds.; Springer-Verlag: Berlin, 1993; Vol. 30, p 111.
- Ripmeester, J.; Ratcliffe, C.; Tse, J. *J. Chem. Soc., Faraday Trans. I* **1988**, *84*, 3731.
- Cho, G.; Moran, L. B.; Yesinowski, J. P. *Appl. Magn. Reson.* **1995**, *8*, 549.
- Kritzenberger, J.; Gaede, H. C.; Shore, J. S.; Pines, A.; Bell, A. T. *J. Phys. Chem.* **1994**, *98*, 10173.
- Neue, G. Z. *Phys. Chem. Neue Folge* **1987**, *152*, 13.
- Driehuys, B.; Cates, G. D.; Miron, E.; Sauer, K.; Walter, D. K.; Happer, W. *Appl. Phys. Lett.* **1996**, *69*, 1668.
- Baranga, A.; Appelt, S.; Romalis, M. V.; Erickson, C. J.; Young, A. R.; Cates, G. D.; Happer, W. *Phys. Rev. Lett.* **1998**, *80*, 2801.
- Albert, M. S.; Cates, G. D.; Driehuys, B.; Happer, W.; Saam, B.; Springer, C. S.; Wishnia, A. *Nature* **1994**, *370*, 199.
- Albert, M. S.; Balamore, D. *Nucl. Instrum. Methods Phys. Res., Sect. A* **1998**, *402*, 441.
- Leduc, M.; Otten, E. *La Recherche* **1996**, *287*, 41.
- Schmidt, D. M.; George, J. S.; Penttila, S. I.; Caprihan, A.; Fukushima, E. *J. Magn. Reson.* **1997**, *129*, 184.
- Patyal, B. R.; Gao, J.-H.; Williams, R. F.; Roby, J.; Saam, B.; Rockwell, B. A.; Thomas, R. J.; Stolarski, D. J.; Fox, P. T. *J. Magn. Reson.* **1997**, *126*, 58.
- Song, Y.-Q.; Gaede, H. C.; Pietrass, T.; Barrall, G. A.; Chingas, G. C.; Ayers, M. R.; Pines, A. *J. Magn. Reson. A* **1995**, *115*, 127.
- Raftery, D.; Long, H.; Meersmann, T.; Grandinetti, P. J.; Reven, L.; Pines, A. *Phys. Rev. Lett.* **1991**, *66*, 584.
- Bowers, C. R.; Pietrass, T.; Barash, E.; Pines, A.; Grubbs, R. K.; Alivisatos, A. P. *J. Phys. Chem.* **1994**, *98*, 9400.
- Pietrass, T.; Gaede, H. C. *Adv. Mater.* **1995**, *7*, 826.
- Bowers, C. R.; Long, H. W.; Pietrass, T.; Gaede, H. C.; Pines, A. *Chem. Phys. Lett.* **1993**, *205*, 168.
- Driehuys, B.; Cates, G. D.; Happer, W.; Mabuchi, H.; Saam, B. *Phys. Lett. A* **1993**, *184*, 88.
- Long, H. W.; Gaede, H. C.; Shore, J.; Reven, L.; Bowers, C. R.; Kritzenberger, J.; Pietrass, T.; Pines, A.; Tang, P.; Reimer, J. A. *J. Am. Chem. Soc.* **1993**, *115*, 8491.
- Rööm, T.; Appelt, S.; Seydoux, R.; Pines, A.; Hahn, E. L. *Phys. Rev. B* **1997**, *55*, 11604.
- Navon, G.; Song, Y.-Q.; Rööm, T.; Appelt, S.; Taylor, R. E.; Pines, A. *Science* **1996**, *271*, 1848.
- Fitzgerald, R. J.; Sauer, K. L.; Happer, W. *Chem. Phys. Lett.* **1998**, *284*, 87.
- Haake, M.; Goodson, B. M.; Laws, D. D.; Brunner, E.; Cyrier, M. C.; Havlin, R. H.; Pines, A. *Chem. Phys. Lett.* **1998**, *292*, 686.
- Solomon, I. *Phys. Rev.* **1955**, *99*, 559.
- Cates, G. D.; Fitzgerald, R. J.; Barton, A. S.; Bogorad, P.; Gatzke, M.; Newbury, N. R.; Saam, B. *Phys. Rev. A* **1992**, *45*, 4631.
- Haake, M.; Pines, A.; Reimer, J. A.; Seydoux, R. *J. Am. Chem. Soc.* **1997**, *119*, 11711.
- Basic Characteristics of AEROSIL. In *Technical Bulletin Pigments*, Degussa: Akron, OH, 1993; Vol. 11.
- Cowgill, D. F.; Norberg, R. E. *Phys. Rev. B* **1972**, *6*, 1636.
- Jeener, J.; Meier, B. H.; Bachmann, P.; Ernst, R. R. *J. Chem. Phys.* **1979**, *71*, 4546.
- Larsen, R. G.; Shore, J.; Schmidt-Rohr, K.; Emsley, L.; Long, H.; Pines, A.; Janicke, M.; Chmelka, B. F. *Chem. Phys. Lett.* **1993**, *214*, 220.
- Brunner, E.; Seydoux, R.; Haake, M.; Pines, A.; Reimer, J. A. *J. Magn. Reson.* **1998**, *130*, 145.
- Pietrass, T.; Seydoux, R.; Pines, A. *J. Magn. Reson.* **1998**, *133*, 299.
- The ratio of transmitted versus incoming intensity, $I(\nu)/I_0(\nu)$, is an exponential function of the inverse absorption length, $\exp(-L/L_\nu)$, where L is the cell length and $1/L_\nu$ is approximately a Lorentz function at the resonance frequency with the pressure broadened width.
- The ^{129}Xe spectra on this sample are very similar to those found on AEROSIL300, although at lower temperatures the line corresponding to adsorbed Xe remains narrower.